Simultaneous Internal/External Flow Calculation of a Solid Fuel Ramjet Projectile: a Design Analysis

Seo Won Choi*, Ho Chul Kang,** Jong Kwan Park** and Sang Kil Lee***

(Received June 28, 1997)

SFRJ has been regarded as a prime mode of secondary propulsion which enables the projectile to achieve a higher terminal velocity. Geometry of SFRJ is quite simple due to the lack of turbomachinery that conventional jet engines need. The complete internal/external flow field of an SFRJ-TGTR projectile at a cruising Mach number is calculated by an unstructured triangular compressible RANSE solver. To complete the analysis, single-component fuel combustion is added in the combustor flow calculation. A commercial CFD package is used with structured rectangular meshes for such computation. The results from the two computations are compared with existing computational and experimental data for validation. The design parameters like thrust, total pressure loss, inlet and nozzle efficiencies and drag coefficient are derived from the detailed flowfield data. Different values of cruising Mach number and nozzle throat area have been tried as a preliminary design procedure. Change in the nozzle throat area directly affects the inlet flow, because the internal flow is mostly subsonic and is linked directly to the nozzle flow.

Key Words: SFRJ (Solid Fuel Ramjet), TGTR (Tank Gun Training Round), KE penetrator (Kinetic Energy penetrator), Internal Flow, External Flow, Oblique Shock, Normal Shock, Choked Flow, Inlet, Combustor, Nozzle, Ratio of Nozzle Throat Area, Coefficient of Drag, Thrust, Total Pressure Loss, RANSE (Reynolds-Averaged Navier-Stokes Equation), Triangular Mesh, Rectangular Mesh, Two-Layer k-ε Model

1. Introduction

The advent of reactive armour places the KE penetrator as the most effective anti-armour projectile. The capability of armour penetration improves as the terminal velocity of the projectile increases. SFRJ can provide the secondary propulsion after the projectile leaves the muzzle to maintain high velocity throughout the flight duration. Therefore it reduces the flight time of projec-

tile and increases the kill probability.

Adaptation of SFRJ projectile does not need any modification to the existing tank cannon system. Ramjet is air-breathing and thus does not need to carry oxidizer. It has a better fuel efficiency at high supersonic regimes than rocket engines, which is a desirable quality for KE weapons. Solid fuel ignites spontaneously right after the projectile leaves the muzzle from viscous heating, and therefore no ignition device is necessary. SFRJ does not have any moving parts so that it provides high structural integrity as well as resilience to rough handlings expected in severe battlefield environments. TGTR is a hollow tubular SFRJ projectile without any penetrator. SFRJ-TGTR is capable of modulating acceleration during the flight such that it provides strong thrust to achieve high supersonic velocity within

*Mechanical Engineering Department, Hong Ik University, Seoul 121-791, Korea

**Graduate School, Hong Ik University, Seoul 121-791, Korea

*** Department of Weapons Engineering, Advanced Institute of Military Science and Technology, Seoul 139-799, Korea

short distances while the fuel is burning. After the end of combustion due to fuel depletion, it becomes a high-drag projectile with sharp deceleration. Such features render SFRJ-TGTR as an ideal training round for KE penetrator, since its ballistics resembles that of KE penetrator in short range where KE penetrator is designed to be effective. However once outside this range the projectile's maximum range is limited by rapid deceleration, which provides the safety feature required of a training ammunition.

Since the ballistics of TGTR closely matches that of KE penetrator, its design can be carried over to the design of KE penetrator without drastic modifications. Especially the recirculation region at the downstream of injector and the nozzle throat ratio can be used directly. For a quick development-type analysis, calculation of external aerodynamics can employ theoretical approaches like Van Dyke's hybrid theory (Van Dyke 1951) and second-order shock expansion theory. (Syvertson and Dennis 1957) Such a study was conducted for both spin-stabilized and fin-stabilized projectiles with various calibers (Sigal and Danberg 1986), and found that a fin-stabilized projectile is unstable for Mach numbers higher than 4 for the particular fin shape tested. The internal flows of three main components, inlet, combustor, and nozzle, are directly linked and affect each other, because SFRJ-TGTR is hollow. An accurate analysis of internal flow and associated combustion process is critical for successfully achieving design goals of flight stability, steady thrust, and structural integrity. To obtain more reliable design analysis, the Navier-Stokes and the Euler computations have been carried out and several results are reported in the literature. (Chakravarthy 1987, Patel and Sturek 1990, Nusca 1989) These attempts included the use of special algebraic turbulence model in the recirculation region of combustor (Chakravarthy 1987), parallel computation with multi-block grids (Patel and Sturek 1990), and a separate internal flow calculation for the resolution of combustion processes. (Nusca 1989) All of them were run on supercomputers due to the size of computations, but none of the calculations, how-

ever, encompass the whole internal/external flow fields. This is partly due to the old and ineffective algorithms used in their computations, i. e. implicit time-integration and zonal grids that are known to give slow convergence for compressible flow calculations.

In this study, a complete field of internal/external flow of an SFRJ-TGTR has been calculated simultaneously by an explicit RANSE solver with two-layer $k-\varepsilon$ turbulence model and a single block grid in several parameter ranges for design analysis. The nozzle throat ratio has been varied to include both oblique and normal shock cases at the inlet. Detailed field variations are shown for all flow variables including turbulence quantities. Also coefficient of drag and total pressure loss in each engine component are given. A computation including combustion processes in the combustor was carried out by a commercial CFD package CFD-ACE. (CFDRC 1993) Mass fraction and temperature profiles are given to indicate the flame locations. Thrust of SFRJ was calculated by applying control volume analysis to the entire computational domain.

These results give sufficient data for preliminary design analysis of a SFRJ-TGTR. The procedure used in this analysis also provides a prototype of consistent design approach completely based on accurate CFD computation in which neither ad hoc empirical rules nor theoretical guidelines with limited applications are used. Since ramjet engines are regarded as the best overall propulsion type for next generation of medium to long range missiles, the proposed design method will enrich the foundation of national ramjet technology.

2. Analysis

The dimensionless, compressible, steady, Reynolds-averaged Navier-Stokes equation can be expressed as

$$\nabla \cdot (\rho u) = 0, \tag{1}$$

$$\nabla \cdot (\rho u \times u) = \nabla \cdot \tau, \tag{2}$$

$$\nabla \cdot (u \rho E) = \nabla \cdot (\tau u) + k \triangle T, \tag{3}$$

where the stress tensor of a Newtonian fluid is

$$\tau = -pI + \mu(\nabla u + \nabla u^t) - \frac{2}{3}\nabla \cdot uI, \qquad (4)$$

and the non-dimensional total energy is defined as

$$E \equiv \frac{|u|^2}{2} + T \qquad (5)$$

The link between pressure and energy is supplied by the equation of state for calorically perfect gas:

$$p = (\gamma - 1)\left(\rho E - \frac{\rho|u|^2}{2}\right) \qquad (6)$$

where γ is the ratio of specific heats. The coefficient of viscosity is assumed to vary with respect to temperature according to Sutherland's law,

$$\mu = \mu_\infty \frac{T_\infty + 110}{T + 110}\left(\frac{T}{T_\infty}\right)^{1.5} \qquad (7)$$

where the subscript ∞ denotes the reference quantities.

The discretization of (1)–(3) gives the following algebraic vector equation,

$$\nabla \cdot [F(W) - N(W)] = S(W). \qquad (8)$$

The vector of dimensionless conservative variables consists of

$$W = [\rho, \rho u, \rho v, \rho E, \ \rho k, \ \rho \varepsilon]^T \qquad (9)$$

F and N are advective and viscous algebraic operators respectively. A second-order upwind MUSCL scheme (Van Leer 1979) is used to construct F. Van Albada type flux limiter (Van Albada and Van Leer 1984) eliminates the dispersion error in the regions near the Euler discontinuities (shock waves). The vector of source terms is

$$S = [0, 0, 0, 0, S_k, S_\varepsilon]^T \qquad (10)$$

Two-layer $k\text{-}\varepsilon$ turbulence model is used where standard $k\text{-}\varepsilon$ with compressibility correction (Sarkar et al. 1991) is employed in high Reynolds number region and a low-Reynolds number $k\text{-}\varepsilon$ model is used in near wall region. The source terms for transport equations of turbulent kinetic energy and rate of dissipation in high-Reynolds number region are expressed as

$$S_k = \mu_t P - \frac{2}{3}\rho k\nabla \cdot \vec{u} - \rho\varepsilon + \overline{p'\nabla \cdot u''} + \frac{\overline{\rho'u''}}{\rho}\nabla p$$

$$S_\varepsilon = c_1\rho k P - \frac{2}{3}\frac{c_1}{c_\mu}\rho\varepsilon\nabla \cdot \vec{u} - c_2\rho\frac{\varepsilon^2}{k}$$
$$+ c_3\frac{\varepsilon}{k}\left[\overline{\rho'\nabla \cdot u''} + \frac{\overline{\rho'u''}}{\rho}\nabla p\right] \qquad (12)$$

The last two terms of Eq. (11) and the last term of Eq. (12) represent the compressibility correction to the standard $k\text{-}\varepsilon$ model. The source term for turbulent kinetic energy is modified in low-Reynolds number region as

$$S_k = \mu_t P - \frac{2}{3}\rho k\nabla \cdot \vec{u} - \rho\frac{k^{3/2}}{l_\varepsilon} + \overline{\rho'\nabla \cdot u''}$$
$$+ \frac{\overline{\rho'u''}}{\rho}\nabla p \qquad (13)$$

where

$$P = \left[\nabla \vec{u} + \nabla \vec{u}^t - \frac{2}{3}I\nabla \cdot \vec{u}\right] \qquad (14)$$

3. Computation

The values of geometric parameters used in this computation is shown in Table 1. The variable nozzle throat ratio determines whether the internal flow will be choked or not, which in turn affects the kind of shock wave taking place at the inlet. The flow parameters are given in Table 2.

The computational grid system is constructed in two steps. Initially body-fitted curvilinear grids are constructed in a multi-block fashion by dividing the domain in six parts, where grid clustering with hyperbolic-tangent function and multi-surface for near-wall grids' orthogonality

Table 1. Geometric parameters of the projectile in calibers.

Inlet diameter	0.608
Injector diameter	0.745
Nozzle throat diameter	0.542 or 0.373

Table 2. Parameter values used in calculation.

	Case I	Case II	Case III	Case IV
Cruising Mach number	4.0	3.0	4.0	3.0
Nozzle throat diameter in cal.	0.373	0.373	0.542	0.542

Fig. 1   Grid system.

Fig. 3   Velocity vectors.

co - freestream   da   symmetric
bc - no reflection   efge - wall
cd - downstream

Fig. 2   Boundary conditions.

Fig. 4   Pressure contours.
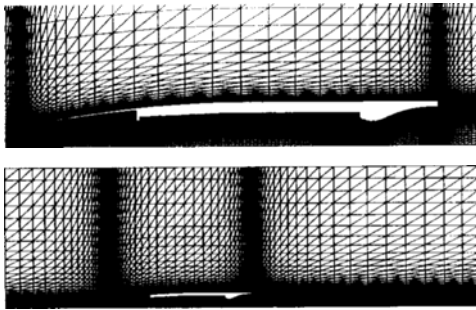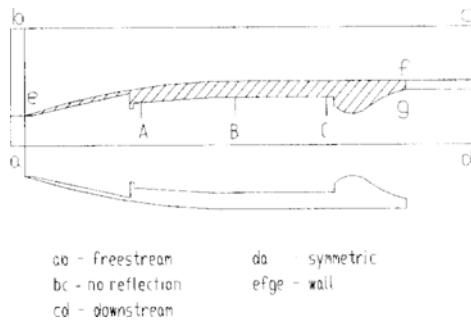

Fig. 5   Mach number contours.

are implemented. Then each rectangular grid is divided into two triangles, and each triangular grids in six parts are all linked to form an approriate connectivity table. Such a grid system for one particular geometry is shown in Fig. 1.This grid system consists of 11,950 triangles and 6,251 vertices. In this way neither we lose spatial accuracies at block interfaces (Chakravarthy 1987) nor have to introduce a special algorithm to take care of interfacial grids. (Patel and Sturek 1990)

As shown in Fig 2, no slip boundary condition is imposed on all solid boundaries, and uniform supersonic flow is specified at the upstream. Symmetry condition is used along the symmetry axis. At the downstream, Dirichlet condition for pressure is imposed while Neumann condition is given for velocity components.

4. Results and Discussion

The velocity vectors in case IV is shown in Fig. 3, where three recirculation regions, cowl, injector step and nozzle exit are identified. The separation and vortex in the combustor is necessary to stabi-
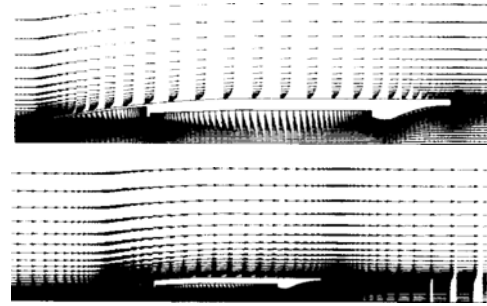
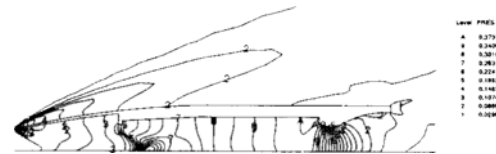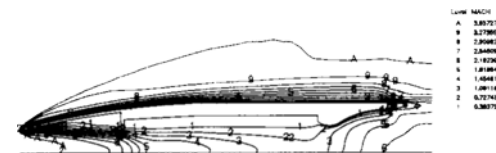lize the flame and improve combustion efficiency. The other two recirculations will only contribute to the overall drag so that geometry modification to reduce the vortex size may be desirable. However reducing the expansion rate of the cross section at inlet and nozzle will both increase the length of the projectile and thus is detrimental to flight stability, for whose analysis a separate study is called for.

Figures 4 and 5 are contour lines of pressure and Mach numbers for the same case. Both internal and external flows include oblique shock waves because case IV has a wide nozzle throat. When nozzle throat becomes narrower to 0.373, i. e. cases I and II, internal flow chokes and normal shock wave takes place at the inlet instead of oblique shock wave. (Patel and Sturek 1990)

The contour lines of turbulent kinetic energy in Fig. 6 show high turbulence level at the combustor, which is created by the injector step intentionally. It also captures the development of turbulent boundary layer in the external flow at the same time. Figure 7 shows the dissipation rate of TKE,
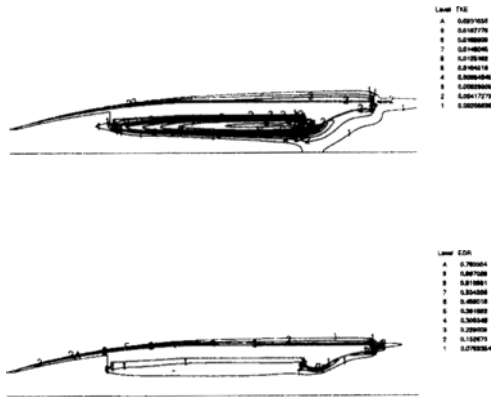
Fig. 7 Contours of rate of dissipation.

Table 3. Total pressure loss in each component. The subscripts 1, 2, and 3 indicate inlet, combustor, and nozzle, respectively.

(in Pascals)	$(\triangle P_T)_1$	$(\triangle P_T)_2$	$(\triangle P_T)_3$
Case I	2238090	242459	1183990
Case II	1645050	114268	636018
Case III	10728100	222112	604158
Case IV	2006690	175127	375688

which is more confined to solid boundaries than TKE itself.

The total pressure losses in each component are shown in Table 3.They are valuable parameters for component design of ramjet engines. The total pressure of the incoming freestream increases as the Mach number increases. Therefore the total pressure losses increase as the Mach number increases.

A control volume analysis is applied to the whole computational domain, and force balance in streamwise direction gives the following equation for drag coefficients:

$$C_D = \frac{2}{\rho V^2 A_{ref}} \left[\iint_{A_1} \rho_1 \vec{V_1}(\vec{V_1} \cdot \hat{n}_1) \, dA - \iint_{A_2} \rho_2 \vec{V_2}(\vec{V_2} \cdot \hat{n}_2) \, dA \right]$$ (15)

where the subscripts 1 and 2 mean the upstream and downstream boundaries respectively. The cross-sectional area of projectile is used for the reference area. The values of drag coefficients are tabulated in Table 4.The coefficients of drag for

Table 4. Coefficients of drag.

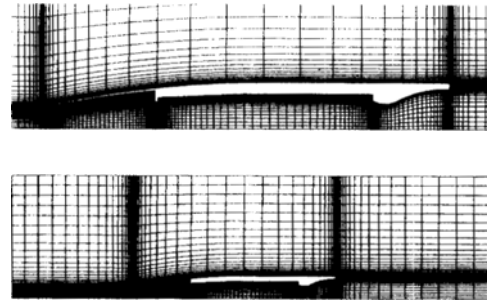|	Case I	Case II	Case III	Case IV
C_D	0.5316	0.5970	0.2544	0.2985

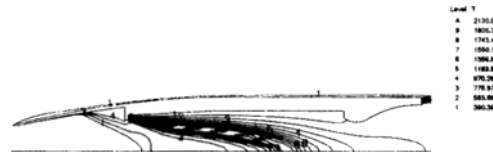**Fig. 8** Computational grids.

Fig. 9 Temperature field with combustion.

cases I and II,with narrower nozzle throat, are higher than those of cases III and IV due to the presence of normal shock wave.

A simultaneous calculations of internal/external flows with combustion were carried out by using a commercial CFD package CFD-ACE (CFDRC 1993). A rectangular grid system is used and is shown in Fig. 8.Combustion processes involved in burning of solid rocket fuels are enormous and the information on reaction rates are far from complete. Therefore the fuel is assumed to be a single species of hydrocarbon. It is also assumed that the reaction occurs in one step and is irreversible. All processes occur in complete thermodynamic equilibrium. The fuel and air are fully consumed in the chemical reaction and they do not coexist at any point in the field. So the reaction is mass-controlled. Also the reaction rate is assumed to be much faster than the rate of diffusion so that the reaction is diffusion-controlled. Therefore no information on reaction rate is necessary to carry out the calculation. Figure 9 shows the contour lines of temperature field. The variations are concentrated in the
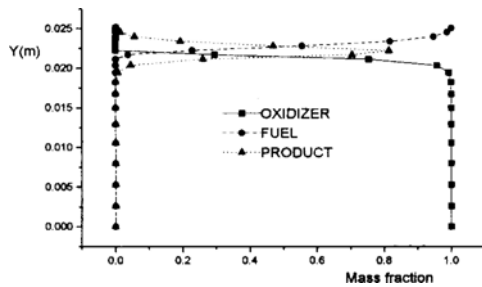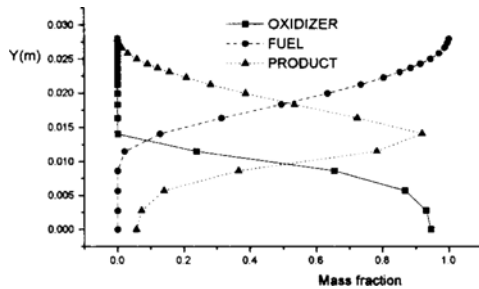
Fig. 10 Mass fractions at A.
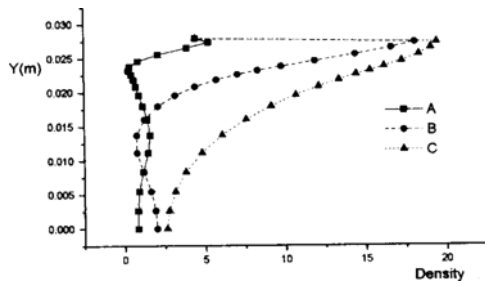

Fig. 11 Mass fractions at B.

Fig. 12 Density profile.

Fig. 13 Temperature profile.

To verify the accuracy of the computation with combustion processes, radial distribution of mass fractions at two different locations inside the combustor are plotted in Figures 10 and 11.(see Fig. 2) These can be compared to the results of Nusca (1989), and the comparison confirms our results. The radial profile of density and temperature at the three locations are shown in Figures 12 and 13, respectively. These plots show the change in flame locations as the flame spreads to the downstream section of the combustor. The thrust of ramjet engine is computed to be 1, 440 N for case III.

In summary, the simultaneous computations of internal/external flows of SFRJ-TGTR were carried out in several parameter ranges. Important design parameters are derived from the detailed flowfield data obtained from RANSE computation. Results were compared with existing computational and experimental data for validation. The methodology employed provides a prototype of consistent design approach completely based on accurate CFD computation in which neither ad hoc empirical rules nor theoretical guidelines with limited applications are used.

References

CFD-ACE: Theory Manual, v1.0, CFDRC, 1993.

Chakravarthy, S. R. 1987, "A New Computational Capability for Ramjet Projectiles," *BRL-CR-595.*

Guidos, B. J. 1990, "External Flow Computations for a Finned 60mm Ramjet in Steady Supersonic Flight," *BRL-MR-3801.*

Nusca, M. J. 1989, "Steady Flow Combustion Model for Solid-Fuel Ramjet Projectiles," *BRL-TR-2987.*

Patel, N. R., Sturek, W. B. 1990, "Parallel Numerical Simulations of Axisymmetric Projectile Flows using Zonal-Overlapped Grids," *BRL-MR-3834.*

Sarkar, S., Erlebacher, G. Hussaini, M. Y., Kreiss, H. O. 1991, "The Analysis and Modelling of Dilatational Terms in Compressible Turbulence," *J. Fluid Mech.,* Vol. 227, pp. 473~493.
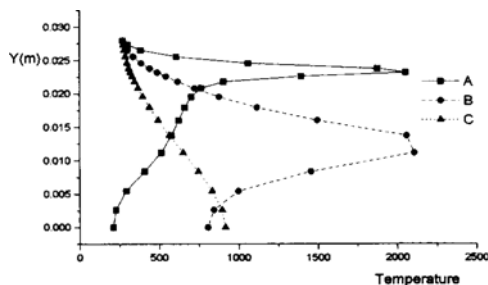
combustor, where the combustion takes place, as well as the downstream of the nozzle exit. The latter region vividly captures the cooling and mixing of the hot exhaust gas with cool ambient air surrounding the jet.

Sigal, A., Danberg, J. E. 1986, "Aerodynamic Analysis of Solid Fuel Ramjet Projectiles," *BRL -MR-3687*.

Syvertson, C. A., Dennis, D. H., 1957, "A Second-Order Shock-Expansion Method Applicable to Bodies of Revolution near Zero-Lift," *NACA Report 1328*.

Van Albada, G. D., Van Leer, B., 1984, "Flux Vector Splitting and Runge-Kutta Methods for the Euler Equations," *ICASE Report 84-27*.

Van Dyke, M. D., 1951, "First- and Second -Order Theory of Supersonic Flow past Bodies of Revolution," *Journal of Aerospace Science,* Vol. 18, No. 3.

Van Leer, B., 1979, "Towards the Ultimate Conservative Difference Scheme V. A Second Order Sequel to Godunov's Method," *J. Comp. Phys.,* Vol. 32, pp101~136.